MODELLING AND OBSERVER-BASED FAULT DETECTION FOR AN AUTOMOTIVE DRIVE-TRAIN

J.A.F. Vinsonneau*, D.N. Shields*, P.J. King†, K.J. Burnham*

* School of Mathematical and Information Science, Coventry University, Coventry CV1 5FB. U.K. Tel: +44 (0)2476 888972, fax: +44 (0)2476 888052, Email: d.n.shields@coventry.ac.uk
† Jaguar Cars Ltd, Coventry, U.K.

Keywords: Drive-train modelling, automotive, nonlinear system, fault detection, observers

Abstract

Observer-based fault detection and modelling are considered for the drive-train of a Jaguar car with an automatic transmission. Test data is used for the modelling and use is made of nonlinear polynomials, where various structures are compared and assessed. A robust fault detection observer (RFDO), consisting of an observer which generates a residual, for the class of nonlinear models emerging from the modelling, is proposed consisting of polynomial nonlinearities up to degree three and a cubic term with respect to the state and input. The observer and the residual are decoupled from unknown inputs. Three fault scenarios are considered, each with a different set of measurements, to test the effectiveness of the RFDO design.

1 Introduction

Automotive emission regulations and the requirement for improved fuel economy have driven innovation in powertrain design and control for more than three decades. Low Emission Vehicle (LEV) II regulations, running from 2004 until 2010, require on-board diagnostics to be more sophisticated, detecting emission problems relating to any sensor or component of the engine [2]. A means of detecting problems early is to make use of a fault detection method based on a system model ([7, 9]). This forms part of the theory of FDI recently introduced in most modern cars to control and diagnose engine malfunctions ([8, 4]). Of the great variety of methods used in the literature where system knowledge is available, the most common is the model-based method for generating residuals and forming decision logic ([3]).

This paper considers improvements in the form of better modelling and a new FDI method for a complete car drive-train. Section 2 considers the modelling of the drive-train of the car. Section 3 develops a RFDO strategy for fault detection. Section 4 is an application of sections 2 and 3. Variables used in this paper are defined in Table 1.

2 Drive-train model development

The modelling of the drive-train of the car is considered. The dynamic equations describing the manifold pressure, the engine speed and the wheel speed are expressed using nonlinear polynomials. Figure (1) shows a realistic Simulink model of the drive-train, which is derived by breaking each of the many dynamic and passive engine components into blocks. Those corresponding to the torque converter, gear box and differential do not have equivalent explicit differential equations for their description. For example, the gear ratio R_{tr} is linked to R_d and W_w through two tables, where one of which is logical in form, and the differential relationship is not that of a simple explicit differential equation. The problem is partly avoided by assuming that R_{tr} is a measured input (since its information is known). Inputs u_5 and u_7 are similarly taken as measured values. In Fig. (1), they are derived from classified control algorithms and are not available in explicit form. Thus, the actual inputs that can be manipulated in Fig. (1) are u_1 and u_4. The car can be driven automatically (simulated) by varying u_1 and u_2. The model in Fig. (1) has been verified to be accurate compared with data collected from road tests. An objective for Jaguar Cars is, assuming Fig. (1) represents now a real car, to determine if a RFDO is effective. Since the Simulink model

	Description	units	scaling units
u_1	Throttle angle, θ	$[deg]$	$u_{1N} = u_1/50$
u_2	Braking force $F_{braking}$	$[kN]$	$u_{2N} = u_2/2.5$
u_3	Mass of car m_{veh}	$[tons]$	$u_{3N} = u_3/2.5$
u_4	Road gradient r_g	$[deg]$	$u_{4N} = u_4/30$
u_5	Spark Advance σ	$[deg]$	$u_{5N} = u_5/50$
u_6	Air/Fuel ratio A/F	$[-]$	$u_{6N} = u_6/26$
u_7	Gear ratio R_{tr}	$[-]$	$u_{7N} = u_7/4$
u_{8N}	$u_{1N}u_{7N}$		
x_1	Manifold pressure P_m	$[bar]$	$x_{1N} = x_1/1$
x_2	Engine speed w_e	$[rad/s]$	$x_{2N} = x_2/500$
x_3	Wheel speed w_w	$[rad/s]$	$x_{3N} = x_3/150$
y_1	Man. press. meas.	$[bar]$	$y_{1N} = y_1/1$
y_2	Engine speed meas.	$[rad/s]$	$y_{2N} = y_2/500$
y_3	Wheel speed meas.	$[rad/s]$	$y_{3N} = y_3/150$
R_d	Ratio of differential	$[-]$	
R_r	Rolling radius	$[m]$	
R_{tr}	Torque ratio of TC	$[-]$	
η_{df}	Efficiency of differential	$[95\%]$	
J_e	Inertia of engine	$[kg.m^2]$	
J_v	Inertia of vehicle	$[kg.m^2]$	
T_e	Torque of engine	$[N.m]$	
T_i	Load torque	$[N.m]$	

Table 1: Nomenclature.

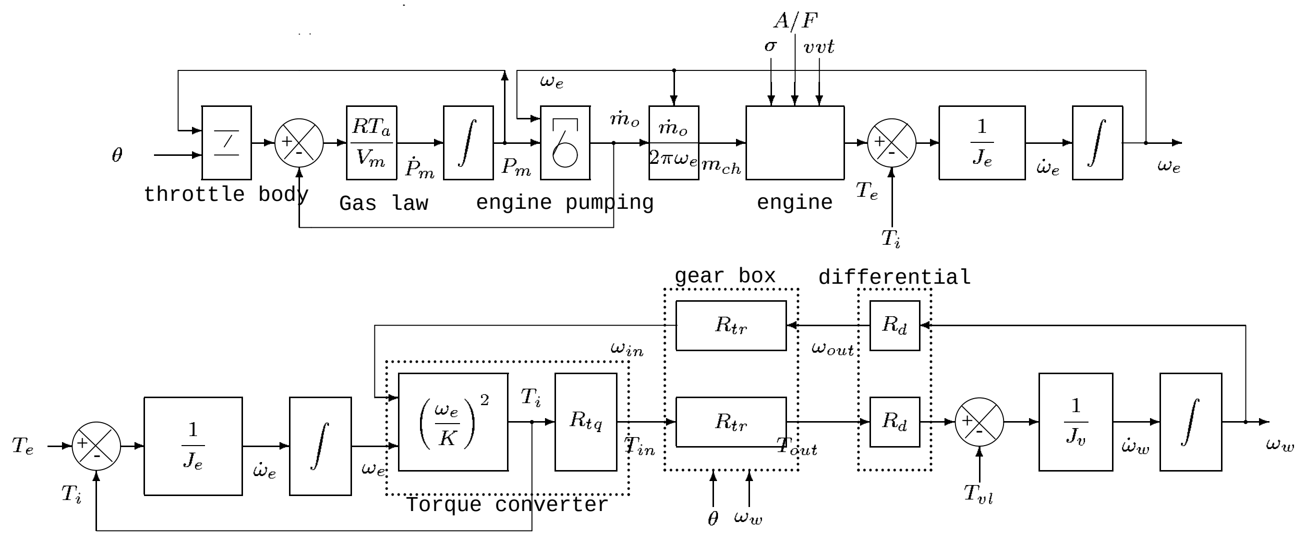

Figure 1: Drive-train diagram of an automatic transmission.

	sx_{1-1}	sx_{1-2}	$\mathbf{sx_{1-3}}$	sx_{1-4}
R_T^2	0.9977	0.9970	**0.9995**	0.8538
IAE	0.0060	0.0065	**0.0024**	0.0495
YIC	-8.2833	-9.4690	**-13.1617**	-1.8389
χ_1^N	x_{1N}	x_{1N}	x_{1N}	x_{1N}
	u_{1N}	u_{1N}	x_{2N}	x_{2N}
	u_{1N}^2	u_{1N}^2	u_{1N}	u_{1N}
	u_{1N}^3	u_{1N}^3	u_{1N}^2	u_{1N}^2
	$x_{2N}x_{1N}$	$u_{1N}x_{1N}$	u_{1N}^3	u_{1N}^3
	$x_{2N}x_{1N}^2$	$u_{1N}x_{1N}^2$	$u_{1N}x_{1N}$	$u_{1N}x_{1N}$
	$x_{1N}x_{2N}^2$	$x_{2N}x_{1N}$	$u_{1N}x_{1N}^2$	
		$x_{2N}x_{1N}^2$	$x_{2N}x_{1N}$	
			$x_{1N}^2x_{2N}$	
			$x_{1N}x_{2N}^2$	

Table 2: Comparison of polynomial structures for (1): $x_{1,N+1} = \chi_1^N\theta_1$.

is not appropriate for observer design, alternative polynomial modelling is considered.

Considered first is the state equation for the manifold pressure, obtained by applying conservation of mass inside the volume of the manifold. The pressure is driven by u_1 and x_2, as shown in [5] and [10] as,

$$\dot{x}_1 = \frac{RT}{V_m}\Big[f(u_1, x_1) - h(x_2, x_1)\Big], \tag{1}$$

where $f(.)$ and $g(.)$ are some nonlinear functions. Equation (1) is discretized. A restricted comparison of modelling structure is shown in Table 2. Parameter vector θ_1 was estimated using a Least-Square (LS) algorithm applied on half of the data set and tested on the full set, where the fitness was assessed using three criteria indices, where χ_1^N is defined in Table 2. Three comparison indices are used to assess the model: the integral-absolute-error (IAE) divided by the number of samples (the smaller the better), the multiple correlation coefficient (R_T^2) (the closer to 1 the better) and the Young Criteria (YIC) (the smaller the better). The structure sx_{1-3} gives better results,

	sx_{2-1}	sx_{2-2}	sx_{2-3}	$\mathbf{sx_{2-4}}$
R_T^2	0.8599	0.8825	0.9019	**0.9632**
IAE	0.0244	0.0249	0.0204	**0.0118**
YIC	-6.5001	-5.3882	-6.9622	**-7.7050**
χ_2^N	x_{2N}	x_{2N}	x_{2N}	x_{2N}
	u_{5N}	u_{5N}	x_{1N}	x_{1N}
	u_{6N}	u_{6N}	$u_{7N}x_{3N}$	x_{1N}^2
	x_{1N}	x_{1N}		$x_{1N}x_{2N}$
	$u_{7N}x_{3N}$	$u_{7N}x_{3N}$		$u_{7N}x_{3N}$
		$u_{7N}x_{3N}^2$		$u_{5N}x_{2N}$
				$u_{5N}x_{2N}^2$

Table 3: Comparison of polynomial structures for (2), $x_{2,N+1} = \chi_2^N\theta_2$.

according to the indices, for which θ_1=[1.014, 0.093,-0.034, 2.163, -1.701, 1.134, -1.451,-0.641, 0.188, -0.289].

The output torque of the engine is characterized by the driving torque T_e resulting from the combustion, and the external load from the torque converter, T_i [5]:

$$\dot{x}_2 = \frac{1}{J_e}\Big[T_e(u_5, u_6, x_1, x_2) - T_i(u_2, u_7, x_2, x_3)\Big] \tag{2}$$

Equation (2) is discretized and fitted with polynomials using a LS algorithm. A restricted set of structures is shown in Table 3. Polynomials structure sx_{2-4} shows the best fit, as indicated by all criteria indices, for which θ_2=[0.968, 0.017, 0.036, -0.118, 0.118, -0.065, 0.243];

The transmission of the torque and revolution speed through the torque converter is expressed by a complex nonlinear relation, due to the fluid coupling [6], and represented in Fig. (1).

$$\dot{\omega}_w = \frac{1}{J_v}\Big[R_d T_{out}\eta_{df} - T_{vl}\Big], \tag{3}$$

with T_{out} the output torque of the gear box. Equation (3) in state form is writtten

$$\dot{x}_3 = \frac{1}{J_v(u_3)}\Big[r(u_7, x_2, x_3) - T_{vl}(u_2, u_3, u_4, x_3)\Big] \quad , \tag{4}$$

	sx_{3-1}	sx_{3-2}	sx_{3-3}	sx_{3-4}
R_T^2	0.8484	0.9879	0.9915	**0.9977**
IAE	0.0447	0.0132	0.0105	**0.0052**
YIC	-5.1696	**-9.0063**	-5.5145	-6.8980
χ_3^N	x_{3N} x_{2N} u_{2N} $u_{2N}x_{2N}$	x_{3N} x_{2N} u_{2N} $u_{2N}x_{2N}$ $u_{2N}x_{3N}$ $u_{7N}x_{3N}$	x_{3N} x_{2N} u_{2N} $u_{2N}x_{2N}$ $u_{2N}x_{3N}$ $u_{7N}x_{3N}$ $u_{8N}x_{3N}$ $u_{8N}x_{2N}x_{3N}$	x_{3N} x_{2N} u_{2N} $u_{2N}x_{2N}$ $u_{2N}x_{3N}$ $u_{7N}x_{3N}$ $u_{8N}x_{3N}$ $u_{8N}x_{2N}x_{3N}$ $u_{8N}^2x_{3N}$ $u_{8N}^2x_{2N}x_{3N}$

Table 4: Restricted comparison of polynomial structures, for system (4).

where $J_v(.)$, $r(.)$ and $T_{vl}(.)$ are nonlinear functions. Equation (4) is discretized and fitted using polynomials. A comparison of stuctures is shown in Table 4. Attention is drawn to structure sx_{3-2}, giving the best polynomial fit with respect to YIC, and also structure sx_{3-4} actually the best fit with respect to both R_T^2 and IAE. Structure sx_{3-4} was therefore selected for which θ_3=[1.000, 0.006, -0.002, 0.004, -0.002, -0.021, -0.137, 0.245, 1.912, -3.662].

Combining models in (1), (2) and (4) together, a compact polynomial model for the SI engine with automatic transmission in derived.

$$\begin{aligned}
\underline{u}_N &= [u_{1N}, u_{1N}^2, u_{1N}^3, u_{2N}, u_{5N}, u_{7N}, u_{8N}, (u_{8N})^2]^T,\\
\underline{x}_{k+1} &= A\underline{x}_k + E_a d_k + K_a f_k + B\underline{u}_k\\
&+ u_k(1)A_{ux}^1\underline{x}_k + u_k(4)A_{ux}^4\underline{x}_k + u_k(5)A_{ux}^5\underline{x}_k\\
&+ u_k(6)A_{ux}^6\underline{x}_k + u_k(7)A_{ux}^7\underline{x}_k + u_k(8)A_{ux}^8\underline{x}_k\\
&+ x_k(1)A_{xx}^1\underline{x}_k\\
&+ u_k(1)x_k(1)A_{uxx}^1\underline{x}_k + u_k(5)x_k(2)A_{uxx}^5\underline{x}_k\\
&+ u_k(7)x_k(2)A_{uxx}^7\underline{x}_k + u_k(8)x_k(2)A_{uxx}^8\underline{x}_k\\
&+ x_k(1)x_k(1)A_{xxx}^1\underline{x}_k + x_k(2)x_k(2)A_{xxx}^2\underline{x}_k, \qquad (5)\\
\underline{y}_k &= C\underline{x}_k + K_s f_k. \qquad (6)
\end{aligned}$$

3 Nonlinear robust fault detection observer

Here, the polynomial model developed in section 2 is used to design a nonlinear full order observer. The work is a development of that in [9] and [1], where different nonlinear models were used. Consider the discrete-time nonlinear model

$$\begin{aligned}
\underline{x}_{k+1} &= A\underline{x}_k + E_a d_k + K_a f_{ak} + B\underline{u}_k\\
&+ \sum_{i_0=1}^{m} u_k^{i_0} A_{ux}^{i_0}\underline{x}_k + \sum_{i_1=1}^{n} x_k^{i_1} A_{xx}^{i_1}\underline{x}_k\\
&+ \sum_{i_0=1}^{m}\sum_{i_1=1}^{n} u_k^{i_0} x_k^{i_1} A_{uxx}^{i_0 i_1}\underline{x}_k + \sum_{i_1=1}^{n}\sum_{i_2=1}^{n} x_k^{i_1} x_k^{i_2} A_{xxx}^{i_1 i_2}\underline{x}_k, \qquad (7)
\end{aligned}$$

$$\underline{y}_k = C\underline{x}_k + K_s f_{sk}, , \qquad (8)$$

with state $\underline{x}_k \in \mathbb{R}^n$, input $\underline{u}_k \in \mathbb{R}^m$, output $\underline{y}_k \in \mathbb{R}^p$ and disturbance $d_k \in \mathbb{R}^q$. Here, A, B, C, K_a, K_s, E_a, $A_{ux}^{i_0}$ $A_{xx}^{i_1}$, $A_{uxx}^{i_0 i_1}$ and $A_{xxx}^{i_1 i_2}$ are constant matrices of appropriate dimensions. A nonlinear state observer is designed, of the form

$$\begin{aligned}
z_{k+1} &= Fz_k + Ju_k + Hy_k + \sum_{i_0=1}^{m} u_k^{i_0} H_{ux}^{i_0}\underline{y}_k\\
&+ \sum_{i_1=1}^{p} y_k^{i_1} H_{xx}^{i_1}\underline{y}_k + \sum_{i_0=1}^{p}\sum_{i_1=1}^{p} u_k^{i_0} y_k^{i_1} H_{uxx}^{i_0 i_1}\underline{y}_k\\
&+ \sum_{i_1=1}^{p}\sum_{i_2=1}^{p} y_k^{i_1} y_k^{i_2} H_{xxx}^{i_1 i_2}\underline{y}_k, \qquad (9)
\end{aligned}$$

where $z_k \in \mathbb{R}^d$ is a linear estimate of Tx_k. A fault detection signal, also called residual, linear in both z_k and y_k, is defined as $\epsilon_k = L_1 z_k + L_2 y_k$, where $\epsilon_k \in \mathbb{R}^{d_0}(\{d_0, d\} \geq 1)$, $L_1 \in \mathbb{R}^{(d_0\times d)}$ and $L_2 \in \mathbb{R}^{(d_0\times d)}$. The observer error is given by $e_k = z_k - Tx_k$. Without loss of generality, it is assumed $C = [I_p \quad 0_{n-p}]$.

Result: Let (10-21) hold true:

$$\begin{aligned}
TA - FT &= HC, &(10)\\
J &= TB, &(11)\\
TE_a &= 0, &(12)\\
L_1T + L_2C &= 0, &(13)\\
H_{ux}^{i_0}C - TA_{ux}^{i_0} &= 0; i_0 = 1, ..., m, &(14)\\
H_{xx}^{i_1}C - TA_{xx}^{i_1} &= 0; i_1 = 1, ..., p, &(15)\\
TA_{xx}^{i_1} &= 0; i_1 = p+1, ..., n, &(16)\\
H_{uxx}^{i_0 i_1}C - TA_{uxx}^{i_0 i_1} &= 0; i_0 = 1, ..., m, i_1 = 1, ..., p, &(17)\\
TA_{uxx}^{i_0 i_1} &= 0; i_0 = 1, ..., m, i_1 = p+1, ..., n, &(18)\\
H_{xxx}^{i_1 i_2}C - TA_{xxx}^{i_1 i_2} &= 0; \{i_1, i_2\} = 1, ..., p, &(19)\\
TA_{xxx}^{i_1 i_2} &= 0; \quad \{i_1, i_2\} = p+1, ..., n, &(20)\\
|\lambda_i(F)| &< 1. &(21)
\end{aligned}$$

Then e_k and ϵ_k are decoupled from d_k and satisfy the form

$$\begin{aligned}
e_{k+1} &= Fe_k + TK_a f_k + W_k(u_k, y_k, f_{ak}) &(22)\\
\epsilon_k &= L_1 e_k + L_2 K_s f_{sk}, &(23)
\end{aligned}$$

where $W_k(u_k, y_k, 0) = 0$ (W_k not detailed here).

The following numerical algorithm is given for solving Equations (10)-(21). For convenience, without loss of generality, the constant matrices in (7- 8) are partitioned as

$$\begin{aligned}
A &= [A_1 \quad A_2], &(24)\\
A_{ux}^{i_0} &= [A_{1ux}^{i_0} \quad A_{2ux}^{i_0}], &(25)\\
A_{xx}^{i_1} &= [A_{1xx}^{i_1} \quad A_{2xx}^{i_1}], &(26)\\
A_{uxx}^{i_0 i_1} &= [A_{1uxx}^{i_0 i_1} \quad A_{2uxx}^{i_0 i_1}], &(27)\\
A_{xxx}^{i_1 i_2} &= [A_{1xxx}^{i_1 i_2} \quad A_{2xxx}^{i_1 i_2}], &(28)
\end{aligned}$$

where $\{A_1, A_{1ux}^{i_0}, A_{1xx}^{i_1}, A_{1uxx}^{i_0 i_1}, A_{1xxx}^{i_1 i_2}\} \in \mathbb{R}^{n\times p}$ and $\{A_2, A_{2ux}^{i_0}, A_{2xx}^{i_1}, A_{2uxx}^{i_0 i_1}, A_{2xxx}^{i_1 i_2}\} \in \mathbb{R}^{n\times(n-p)}$.

Matrix T is also partitioned into the form

$$T = [T_1 \quad T_2] \tag{29}$$

where $T_1 \in \mathbb{R}^{d\times p}$ and $T_2 \in \mathbb{R}^{d\times(n-p)}$. The equations (10), (13), in addition to (14), (15), (17) and (19) are correspondingly partitioned into the form

$$TA_1 - FT_1 = H \tag{30}$$
$$TA_2 - FT_2 = 0 \tag{31}$$
$$L_1T_1 - L_2 = 0 \tag{32}$$
$$L_1T_2 = 0 \tag{33}$$
$$TA_{1ux}^{i_0} = H_{ux}^{i_0} \tag{34}$$
$$TA_{2ux}^{i_0} = 0; i_0 = 1, ..., m \tag{35}$$
$$TA_{1xx}^{i_1} = H_{xx}^{i_1} \tag{36}$$
$$TA_{2xx}^{i_1} = 0; i_1 = 1, ..., p \tag{37}$$
$$TA_{1uxx}^{i_0 i_1} = H_{uxx}^{i_0 i_1} \tag{38}$$
$$TA_{2uxx}^{i_0 i_1} = 0; i_0 = 1, ..., m, i_1 = 1, ..., p \tag{39}$$
$$TA_{1xxx}^{i_1 i_2} = H_{xxx}^{i_1 i_2} \tag{40}$$
$$TA_{2xxx}^{i_1 i_2} = 0; \{i_1, i_2 = 1\}, ..., p \tag{41}$$

Equations (31), (35), (37), (39) and (41) can be merged into one equation,

$$T[A_{2ux}^{i_0}, A_{2xx}^{i_1}, A_{2uxx}^{i_0 i_1}, A_{2xxx}^{i_1 i_2}, E_a] = TZ = 0 \tag{42}$$

Matrix T is solved in (42) as $\begin{bmatrix} T_1 & T_2 \end{bmatrix} = MU_{z2}^T$, where U_{z2} is obtained from the SVD of Z,

$$Z = \begin{bmatrix} U_{z1} & U_{z2} \end{bmatrix} \begin{bmatrix} \Sigma_{z1} & \\ & 0 \end{bmatrix} \begin{bmatrix} V_{z1} & V_{z2} \end{bmatrix}^T, \tag{43}$$

and M is an arbitrary $d \times r$ matrix with r, the order of the left null space for Z, being given as

$$r = n - rank\{Z\}, \tag{44}$$

where $r \geq 1$ is needed. The observer order, d, is chosen as $d = r$. U_{z2}^T is partitioned into two matrices

$$U_{z2}^T = \begin{bmatrix} N_1 & N_2 \end{bmatrix}, \tag{45}$$

where $N_1 \in \Re^{r\times p}$ and $N_2 \in \Re^{r\times(n-p)}$. Then equation (29) is equivalent to the following two equations $T_1 = MN_1$ and $T_2 = MN_2$. If the following conditions are satisfied,

$$TA_2(I_n - T_2^+ T_2) = 0, \tag{46}$$
$$MU_{z2}^T A_2 \big(I_n - (MN_2)^+ (MN_2)\big) = 0, \tag{47}$$

the observer matrix F has the following general form such that (31) is satisfied,

$$F = TA_2(T_2)^+ \tag{48}$$
$$= MU_{z2}^T A_2 (MN_2)^+ + W\big(I_d - MN_2(MN_2)^+\big) \tag{49}$$
$$= A^* + WC^*, \tag{50}$$

where W is a $d \times d$ arbitrary matrix. The eigenvalues of W are designed such that R is stable. $(.)^+$ represents the pseudo inverse of $(.)$.

The matrix H is calculated from (30) and J from (11). Equations (32) and (33) have solutions,

$$L_1 = W_1 U_{n2}^T, \; L_2 = -L_1 T_1, \tag{51}$$

where U_{n2} is from the SVD of T_2

$$T_2 = \begin{bmatrix} U_{n1} & U_{n2} \end{bmatrix} \begin{bmatrix} \Sigma_n & \\ & 0 \end{bmatrix} \begin{bmatrix} V_{n1} & V_{n2} \end{bmatrix}^T, \tag{52}$$

where W_1 is a$\Phi \times r_n$, chosen arbitrary, with

$$r_n = d - rank\{T_2\} \geq d - (n-p). \tag{53}$$

The dimension of the residual vector is chosen $\Phi = r_n$. Given d, Φ, T, F, L_1 and L_2, the matrices J, H, $H_{ux}^{i_0}$, $H_{xx}^{i_1}$, $H_{uxx}^{i_0 i_1}$ and $H_{xxx}^{i_1 i_2}$ are obtained from (30), (32), (34), (36) (38) and (40).

Detectability: In order that ϵ_k is affected by faults, the following sufficient conditions are deriveable,

$$L_1 F^i T K_a \neq 0, \quad \forall\, i,\; i \leq d,\; (f_{ak} \neq 0, f_{sk} = 0)$$
$$L_1 F^i W_k \neq 0, \quad \forall\, i,\; i \leq d,\; \forall k (f_{ak} = 0, f_{sk} \neq 0)$$

Remark: The size of Z increases with respect to the complexity of the system. The freedom for obtaining robustness of the RFDO decreases with the increase of the number of the nonlinear terms.

4 Applications

For models (1) and (2), data was taken from an Jaguar car model "XJ8 Saloon", normally aspirated 4 litre, V8 engine, automatic gearbox, for a general driving cycle and with normal atmospheric conditions, and temperature. The sampling rate was 50ms. Data for (4) was partially simulated in Simulink as some real data was lacking (gear selection, braking force).

4.1 Computational algorithm

The flow-chart in Fig. 2 represents the computational algorithm described in Section 3. Three classes of output, with $p < n$, are considered: for each, $n = 3$, $p = 2$ and $E_a = 0$. The form of C affects the partition of matrices A, B, A_{ux}, A_{xx}, A_{uxx} and A_{xxx}, and thus the constructed matrix Z.

Class 1: only x_1 and x_2 measured. $y = [x_1 \quad x_2 \quad 0]'$. For this case, in (42), $rank\{Z\} = 2$ and the observer and residual can be designed.

Class 2: only x_2 and x_3 measured. $y = [x_2 \quad x_3 \quad 0]'$. For this case, in (42), $rank\{Z\} = 2$ and the observer and residual can be designed.

Class 3: only x_1 and x_3 measured. $y = [x_3 \quad x_1 \quad 0]'$. Here, (42) and (44) imply an observer cannot be designed. A novel recovery solution is proposed for this (see Fig. 2). It consists of reducing the rank of Z by resetting (judiciously) certain coefficients in the matrices in (42). This hopefully ensures $r > 0$ and a residual can be designed. The downside is that the designed

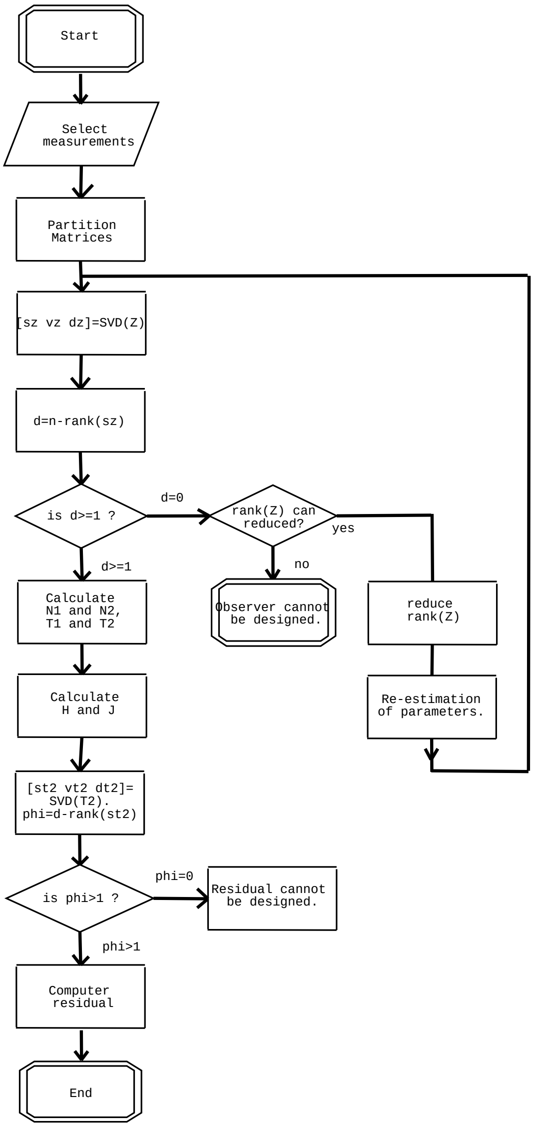

Figure 2: flowchart for RFDO.

residual is affected by an increase in modelling error. For the application here it is seen that

$$Z = \begin{bmatrix} 0 & 0.0036 & 0 & 0 & 0 & 0 & 0 & \ldots \\ 0 & 0 & 0 & 0 & 0 & 0 & -0.6413 & \ldots \\ 0 & 0 & -0.0477 & 0 & 0 & 0 & -0.2419 & \end{bmatrix}$$

$$\begin{matrix} & 0 & 0 & 0 & 0 & 0 & 0 & 0 \\ \ldots & 0 & 0 & 0 & 0 & 0.1887 & 0 & 0 \\ & 0 & 0.2222 & 0 & 0 & 0 & 0 & 0 \end{matrix}\Bigg] \quad (54)$$

In equation (54), $Z_{(1,2)}$ is the only element in row 1, and is identified as $\theta_3(4)$. The latter is reset and θ_3 refitted as in Table 4 as $\theta_3^{'}$=[1.0004, 0.0046, -0.0007, **0**, -0.0023, -0.0180, -0.1043, 0.1825, 2.1824, -4.207]. Then $rank\{Z\} = 2$ and from (44), $r = 2$.

For all classes the approximation of the model by a polynomial leads to some modelling error and offset. The modelling error here is considered as noise and is filtered with a low-pass filter. An offset is inevitable, however, and will not vanish. Its amplitude can be estimated from the mean value of non-faulty residuals, as shown in Table 5. An offset is here subtracted from the corresponding residual.

Outputs	ϵ	mean value of residuals (offset)
y_1, y_2	$\bar{\epsilon}_{12}$	-2.4991e-5
y_2, y_1	$\bar{\epsilon}_{21}$	+2.4991e-5
y_1, y_3	$\bar{\epsilon}_{13}$	-0.0135
y_3, y_1	$\bar{\epsilon}_{31}$	+0.0135
y_2, y_3	$\bar{\epsilon}_{23}$	-5.9247e-4
y_3, y_2	$\bar{\epsilon}_{32}$	-5.9247e-4

Table 5: Offset for residuals for different classes of y.

4.2 Results

For each class described in section 4.1, the construction of Z leads to a first order observer. Condition (13) is satisfied, and (53) holds for each case.

Three multiplicative sensors faults were created on measurement, with an amplitude of 30%. f_1^s was added to y_{1N} for $t \in [50 : 150]$, f_2^s to y_{2N} for $t \in [200 : 300]$, and f_3^s to y_{3N} for $t \in [400 : 500]$ as shown in Fig. 3. A leak, a component fault f_1^a, corresponding to a hole ($\varnothing 3mm$) in the manifold and an actuator fault f_2^a, corresponding to a loss of 50Nm in the torque converter were also simulated in a Simulink environment, where the Simulink model was taken as the real car. Modified data was saved to a file. f_1^a and f_2^a were applied for $t \geq 500$, as represented in Fig. 3. The mean value was taken off, $\breve{\epsilon} =| \epsilon - \bar{\epsilon} |$, where $\bar{\epsilon} =$*mean value* (off-set). Then ϵ_1 was filtered using a low-pass filter with a cut-off frequency at 1Hz, to attenuate high frequency effects due to bad modelling. The level of thresholds were fixed at 5% of each sensor fault. Figure 4 shows the non-faulty measured scaled value for the manifold pressure, the engine speed and the wheel speed.

Scenario 1: class 1 and residual ϵ_{12}. Two sensor faults f_1^s, f_2^s and an actuator fault, f_1^a are applied. Fig. 5 (top) shows the residual after computation, which responds to both sensor faults and the leak. However, the leak is not always detected, especially for low engine speeds and high manifold pressures, where modelling noise masks the fault.

Scenario 2: class 3 and residual ϵ_{13}. Two sensor faults f_1^s, f_3^s and an actuator fault, f_1^a are applied. In Fig. 5 (middle), the observer aims to estimate the engine speed using y_3. Modelling errors are too big and the leak cannot be detected. The residual responds to f_3^s, but not to f_1^s. A spike appears at $t = 200s$. This is not caused by a fault but is a wrong-flagging (caused by modelling error).

Scenario 3: class 2 and residual ϵ_{23}. Here, f_2^s, f_3^s and f_2^a are applied. Fig. 5 (bottom) shows the response of the residual. A spike appears due to modelling error at time $t = 200s$ (not caused by a fault). Evidence shows that f_3^s $(400 \leq t \leq 500)$ and f_2^a $(t > 500s)$ are detected for high wheel and engine

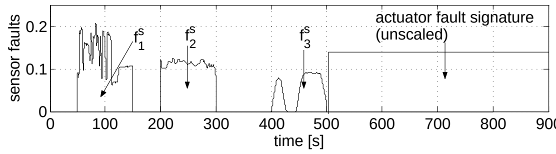

Figure 3: Sensor faults signature.

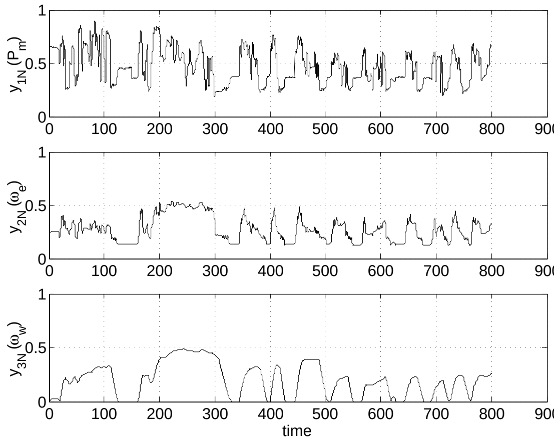

Figure 4: Outputs measured.

speeds. The rersidual is oscillatory in nature for $t > 500$.

Comments on Fig. 5. The horizontal lines indicated are not threshold lines but are placed for readability. For senario 1 the effect of modelling error is smaller and all faults are detecable. For senarios 2 and 3 the effect of modelling error is much larger, deemed mainly due to unmodelled nonlinearities within the torque converter, thus contributing to spikes in the residuals (t=200s). The residual performances shown are the same for other data sets.

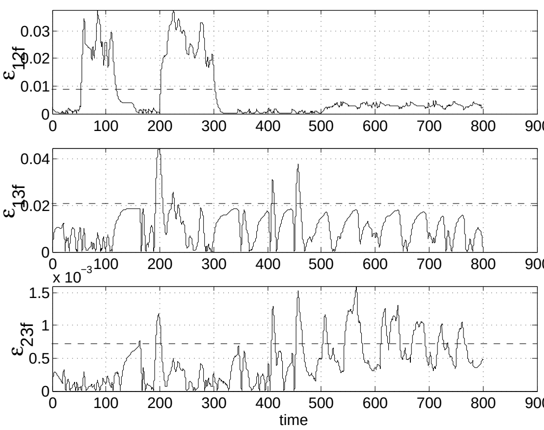

Figure 5: Filtered $\breve{\epsilon}_{12}$, $\breve{\epsilon}_{13}$ and $\breve{\epsilon}_{23}$, respectively ϵ_{12f}, ϵ_{13f} and ϵ_{23f}. ($\breve{\epsilon}_{12} = \mid \epsilon_{12} - \bar{\epsilon}_{12} \mid$, $\breve{\epsilon}_{13} = \mid \epsilon_{13} - \bar{\epsilon}_{13} \mid$ and $\breve{\epsilon}_{23} = \mid \epsilon_{23} - \bar{\epsilon}_{23} \mid$).

5 Conclusions

Effective modelling is shown by using real data, using polynomial nonlinearities and using a judicious relabelling of certain quantities as known measured inputs. Theory for residual design is given for a discretized drive-train model, including a novel design modification. The application of the design theory to a Jaguar car shows the importance of accurate modelling. Three fault senarios, each with a different output class ($p < n$), are considered and residuals are generated for five faults (not simultaneous). Originality of the work consists in improved modelling and a new FDI design for systems of the from (5). The RFDO here can be used to isolate faults, as in [9], using a bank of observers.

References

[1] Sharon Ann Ashton. *Methods for Fault Detection and Isolation With Application to Hydraulic Pipelines*. PhD thesis, Coventry University, Dec 1999.

[2] Jeffrey A. Cook, Jing Sun, and J. W. Grizzle. Opportunities in automotive powertrain control applications. *Proceedings of the 2002 IEEE International Conference on Control Applications*, 2002.

[3] P. M. Frank, S. X. Ding, and B. Köppen-Seliger. Current developments in the theory of FDI. In *IFAC Fault Detection, Supervision and Safety for Technical Processes*, pages 16–27, Budapest, Hungary, 2000.

[4] R. Isermann. Diagnosis methods for electronic controlled vehicles. *Vehicle Systen Dynamics*, 36(2-3):77–117, 2001.

[5] U. Kienche and L. Nielsen. *Automotive Control System - For Engine, Driveline and Vehicle*. Springer-Verlag, Berlin, Germany, first edition, 2000.

[6] G. Lechner and H. Naunheimer. *Automotive Transmissions - Fundamentals, Selection, Design and Application*. Springer-Verlag, Berlin, Germany, first edition, 1999.

[7] R. J. Patton and J. Chen. Observer based fault detection and isolation: Robustness and applications. *Control Engineering Practice*, 5(5):671–682, 1997.

[8] G. Rizzoni, Y. Kim, and A. Soliman. Estimation problems in engine control and diagnosis. In *SAFEPROCESS'00*, pages 124–130, 14-16 June, Budapest, Hungary, 2000. IFAC.

[9] D. N. Shields, S. A. Ashton, and S. Daley. Design of nonlinear observers for detecting fault in hydraulic subsea pipelines. *Control Engineering Practice*, 9:pp. 297–311, 2001.

[10] J. A. F. Vinsonneau, D. N. Shields, P. J. King, and K. J. Burnham. Improved SI engine modelling techniques with application to fault detection. In *Proc. of the IEEE Int. Conference on Control Applications*, Sept. 18-20, Glasgow, Scotland, UK., 2002.